Electrochimica Acta 118 (2014) 26–32

Contents lists available at ScienceDirect

Electrochimica Acta

journal homepage: www.elsevier.com/locate/electacta

Au Electrodeposition at the Liquid-Liquid Interface: mechanistic aspects

Akihiro Uehara [a,b,*], Teruo Hashimoto [c], Robert A.W. Dryfe [a,*]

[a] School of Chemistry, University of Manchester, Oxford Road, Manchester, M13 9PL, United Kingdom
[b] Division of Nuclear Engineering Science, Research Reactor Institute, Kyoto University, Asashironishi, Kumatori, Osaka, 590-0494, Japan
[c] School of Materials, University of Manchester, Oxford Road, Manchester, M13 9PL, United Kingdom

ARTICLE INFO

Article history:
Received 27 September 2013
Received in revised form
29 November 2013
Accepted 29 November 2013
Available online 11 December 2013

Keywords:
Electron transfer voltammetry
ITIES
Au nanoparticle
Tetrachloroaurate
Dichloroaurate

ABSTRACT

The deposition mechanism of metallic gold was investigated based on charge transfer voltammetry at the water/1,2-dichloroethane (W/DCE) interface, and the corresponding redox voltammetry of the metal precursor in W and the reductant, triphenylamine (TPA), in DCE. The metal precursor was present as Au(III) ($AuCl_4^-$), or Au(I) ($AuCl_2^-$) in W or DCE. Electron transfer could be observed voltammetrically at the interface between W containing both Au precursors and DCE containing TPA. Au particles, formed by constant potential electrolysis at the W/DCE interface, were examined by transmission electron microscopy. It was shown that deposit size could be controlled via the applied potential and time, with specific conditions to form particles of less than 10 nm identified.

1. Introduction

The combination of nanotechnology with chemistry, biology, physics, and medicine for the development of ultrasensitive detection and imaging methods in the analytical or biological sciences is becoming increasingly important. Nanoparticle synthesis, at or near the interface between two immiscible liquids has been known since the time of Faraday [1] but it is only in the last two decades or so, with the advent of appropriate microscopic characterization, that the systematic investigation of the relationship between particle size and growth conditions has become more established. A huge variety of nanoparticles has been synthesized, with immiscible liquids frequently used in synthesis [2]. The deposition process at an interface between two immiscible liquids can be considered as an intermediate case between purely homogeneous deposition through electron transfer between redox couples in the same phase, which as a spontaneous process is difficult to control, and heterogeneous deposition at the (conventional) solid electrode-electrolyte interface [3]. Separation of the two reactants, the oxidised metal precursor and a reducing agent, by the liquid-liquid interface means the driving force of nucleation can be controlled through the interfacial potential.

In fact, the electrochemical synthesis of nanoparticles at liquid-liquid interfaces is a relatively new field of research. Charge (electron and ion) transfer reactions at the two immiscible electrolyte solutions have been studied extensively using simple reversible systems, whereas electrochemical synthesis has only been described in a limited number of cases.

The potential controlled electrodeposition of various metals, e.g. Au [4–10], Cu [11], Pd [12–16], Pt [15–17], and Ag [18–22] has been investigated at organic-water interfaces. Other studies of the spontaneous growth process have been carried out using the interfacial potential established through spontaneous transfer of a partitioning ion between the water and organic phases (Nernst partition equilibrium) [12,16,22,23]. Characterization of the initial nucleation process was a focus of some of this work [12]. In order to apply to the formation of nanoparticles, it is important to rationalise the deposition process in terms of existing models of phase formation. To this end, some results for the deposition of metallic Pd at the liquid-liquid interface by a reductant in organic solution have been reported [12,13,15,16,24,25], whereas deposition of metallic gold at the liquid-liquid interface was limited because of the large differences in redox potential between Au ion and reductants [4,6,7]. Furthermore, precise experimental control over nanoparticle size via the potential applied to the liquid-liquid interface has not been described to date, although deposition at the interface has been probed by UV-Vis and X-ray absorption spectroscopy [26]. To prevent nanoparticle aggregation, tetraalkylammonim halides such as cetyltrimetylammonium bromide, CTAB, and tetraoctylammonium

* Corresponding author. Tel.: +81 724 51 2454.
E-mail addresses: auehara@rri.kyoto-u.ac.jp (A. Uehara), robert.dryfe@manchester.ac.uk (R.A.W. Dryfe).

0013-4686/$ – see front matter © 2013 Published by Elsevier Ltd.
http://dx.doi.org/10.1016/j.electacta.2013.11.162

chloride, TOACl, have been widely used as the capping ligands forming monolayers on particle surfaces [27–29]. Cunnane and co-workers [5,9,10] have previously investigated the effect of deposition conditions for the case of Au deposition at the liquid-liquid interface. In their work, Au was not reduced heterogeneously via an organic phase electron donor, rather the $AuCl_4^-$ was transferred from the organic phase to the aqueous phase. Following transfer, the $AuCl_4^-$ underwent a spontaneous homogeneous reduction with an aqueous phase electron donor to form a gold-polymer composite. Both tyramine and resorcinol were used as the electron donors, and the influence of solution pH and applied interfacial potential were investigated. An approximately linear relation between particle diamater (in the range 17 to 35 nm) was found with applied potential, although it is not clear if the Nernst equilibrium included the effect of the $AuCl_4^-$ ion distribution in this case.

In the present study, Au deposition at the water/1,2-dichloroethane (W/DCE) interface was performed with $AuCl_4^-$ and dichloroaurate ($AuCl_2^-$) dissolved in either W or DCE. The Au precursors react at the interface with a hydrophobic amine reductant, triphenylamine, dissolved in DCE, which results in the reduction of $AuCl_4^-$ and $AuCl_2^-$ to form metallic Au. Au deposition at this interface is a relatively complex process. In spite of the interest in Au nanoparticle synthesis at liquid-liquid interfaces, there are few electrochemical studies of Au interfacial deposition. Here, charge (electron and ion) transfer was observed by voltammetry at the W/DCE interface to probe the deposition mechanism. Furthermore, the Au deposit was analyzed by transmission electron microscopy and the effect of the applied potential at the interface and the duration of the electrolysis was investigated.

2. Experimental

2.1. Chemicals

Hydrogen tetrachloroaurate, $HAuCl_4\,3H_2O$ (Alfa, ≥ 99.999%) was used as the source of Au(III), tetrabutylammonium dichloroaurate, $TBA^+AuCl_2^-$ (Tokyo Kasei, ≥ 99.99%) was used as the Au(I) source. HCl was used as a supporting electrolyte. 1,2-dichloroethane, DCE (≥ 99%, Aldrich) was used as the organic solvent. Triphenylamine (TPA, ≥ 99%, Acros Organics) was used as reductant in DCE. The tetraoctylammonium (TOA^+) salt of $AuCl_4^-$ in DCE was prepared by shaking an equimolar volume of $HAuCl_4$ in W and TOA^+Cl^- in DCE for the $TOA^+AuCl_4^-$ case. The TOA^+salt of $AuCl_2^-$in DCE was prepared by shaking pure W with equimolar amounts of $TBA^+AuCl_2^-$ and TOA^+Cl^- in DCE. The supporting electrolyte in DCE for potential sweep experiments was TOA^+TFPB^- or $BTPPA^+TFPB^-$, where $BTPPA^+$ and $TFPB^-$ denote bis(triphenylphosphoranylidene) ammonium cation and tetrakis[3,5-bis(trifluoromethyl)phenyl] borate anion, respectively. $BTPPA^+TFPB^-$ was obtained as a precipitate after mixing a methanol solution of $BTPPA^+Cl^-$ with a methanol solution of Na^+TFPB^-, and was purified by recrystallization from ethanol based on the temperature dependence of the solubility of the salt.

2.2. Measurement of the voltammogram for charge transfer at the macro and micro W/DCE interfaces

Two electrochemical cells were employed; a macro-interface cell and a micro-interface cell. In the (conventional) macro-interface case, cyclic voltammetry experiments were performed using a four electrode configuration with an IVIUM potentiostat ("Compactstat" model, IVIUM Technologies, the Netherlands). No iR compensation was applied for the electrochemical measurements: it was assumed that a sufficient concentration of supporting electrolytes was present in both phases. Homemade Ag/AgCl and platinum gauze were used, respectively, as reference electrodes (RE) and counter electrodes (CE). The organic CE was insulated from the W phase by coating its contact in a glass sheath.

The cell used for the electrochemical measurements at the W/DCE interface had a cross-sectional area of about 0.64 cm^2 and had a volume of 3 cm^3. Further details are described elsewhere [7]. The micro-interface cell uses a 16 μm thick polyester film, with a micro hole 30 μm in diameter, to separate the W and DCE phases [30–32].

The potential difference at the W/DCE interface, E, was measured *vs* the potential of a silver-silver chloride electrode, SSE, in W referred to the potential of a $BTPPA^+$ ion selective electrode [33], inserted in DCE. The generic cell composition is:

Ag | AgCl | 10 mM LiCl (W) | W1 (W) || DCE1 (DCE) | 10 mM $BTPPA^+TFPB^-$ (DCE) | 1 mM $BTPPA^+Cl^-$ + 10 mM LiCl (W) | AgCl | Ag

The E is related to the Galvani potential difference, $\Delta^W_{DCE}\phi$, as.

$$E = \Delta^W_{DCE}\phi + E_{ref} \quad (1)$$

where E_{ref} is the potential of the reference electrodes employed. In the calculation of $\Delta^W_{DCE}G^o(= -zF\Delta^W_{DCE}\phi^o$, the measured E was converted using the extrathermodynamic assumption of Parker [34]. Cell compositions used in this work were summarised in Table 1.

2.3. Electrochemical deposition

Electrochemical deposition was performed using a constant potential for a defined time: the DCE was then separated from W and stored in a glass vial. Immediately prior to transmission electron microscopy, TEM (JEM-2000FX II, JEOL), DCE was dropped on to the TEM grid (Holey carbon films on 300 mesh grids, Agar Scientific) to isolate the deposit.

3. Results and discussion

3.1. Electrochemical reaction between Au species and TPA

3.1.1. Voltammetry of Au deposition using $AuCl_4^-$ dissolved in W

Initially, voltammograms were recorded using W containing $AuCl_4^-$ and supporting electrolyte, and DCE solution without reductant (TPA) to confirm the effect of the latter on the interfacial charge transfer process. Curve 1 in Fig. 1 shows the voltammogram for the transfer of $AuCl_4^-$ between W and DCE. The transfer reaction for the positive and negative current, I_{p1} and I_{n1}, is quasi-reversible and the mid-point potential is calculated to be 0.115 V (Eq. (2)).

$$AuCl_4^-{}_{(DCE)} \rightleftharpoons AuCl_4^-{}_{(W)} \quad (2)$$

Table 1
Cell compositions used in this work.

W1	DCE1	
0.2 mM $HAuCl_4$	10 mM TOA^+TFPB^-	Cell 1
10 mM HCl		Fig. 1
0.5 mM $HAuCl_4$	20 mM TPA	Cell 2
10 mM HCl	10 mM TOA^+TFPB^-	Fig. 2, 4
0, 0.1, 0.2, 0.4 mM	20 mM TPA	Cell 3
$HAuCl_4$	1 mM TOA^+TFPB^-	Fig. 5
10 mM HCl		
10 mM HCl	0.5 mM $TOA^+AuCl_4^-$	Cell 4
	10 mM TOA^+TFPB^-	Fig. 6(a)
10 mM HCl	0.5 mM $TOA^+AuCl_4^-$	Cell 5
	20 mM TPA	Fig. 6(b)
	10 mM TOA^+TFPB^-	
10 mM HCl	0.5 mM $TOA^+AuCl_2^-$	Cell 6
	10 mM TOA^+TFPB^-	Fig. 7(a)
10 mM HCl	0.5 mM $TOA^+AuCl_2^-$	Cell 7
	20 mM TPA	Fig. 7(b)
	10 mM TOA^+TFPB^-	

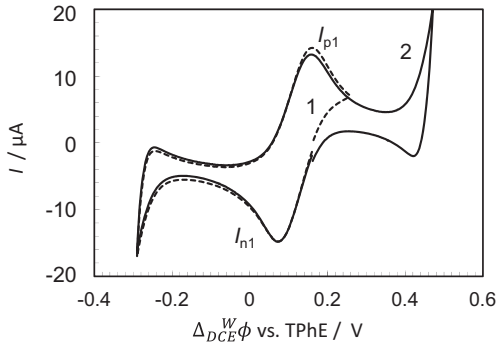

Fig. 1. Ion transfer voltammogram of $AuCl_4^-$ in the absence of TPA in DCE (Cell 1), curve 1: −0.3 to 0.48 V, curve 2: −0.3 to 0.26 V. Scan rate; 20 mV s^{-1}.

The current at the negative vertex (—0.30 V) corresponds to the transfer of Cl^- from the supporting electrolyte between W and DCE. Scans to more positive potentials than 0.24 V, as in curve 2 in Fig. 1, did not yield any current other than the transfer of H^+ present in W as the supporting electrolyte.

On addition of TPA to DCE, the voltammogram shown in Fig. 2 (a) was recorded. When the potential was scanned to 0.26 V, ion transfer of $AuCl_4^-$ between W and DCE was observed, which is similar to the result in the absence of TPA in DCE shown in Fig. 1. However, when the potential was scanned to 0.5 V, the new positive and negative current features, I_{p2}, I_{p3} and I_{n2}, at 0.02, 0.36 and −0.2 V, respectively, were observed as seen in Fig. 2(b). The currents depended on the number of scans. The black curve of the voltammogram is the 1st scan, and the dotted line is the 10th scan. I_{p1} and I_{n1}, corresponding to the transfer of $AuCl_4^-$ between W and

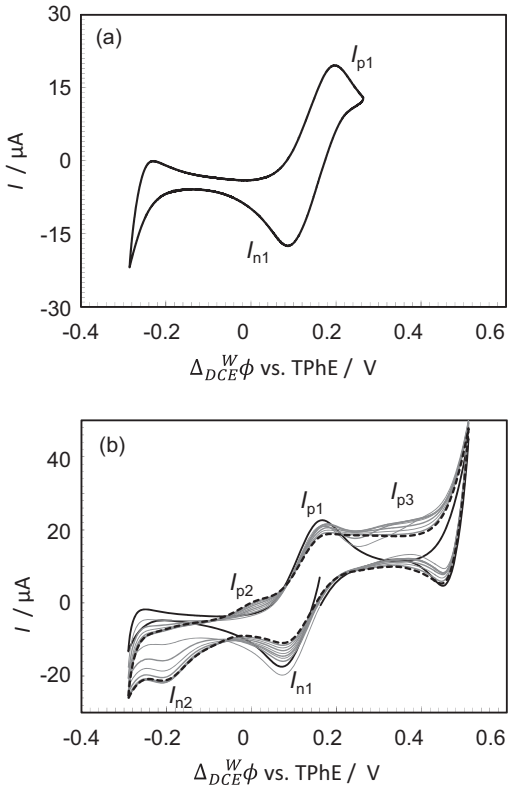

Fig. 2. Charge transfer voltammogram at the macro-interface between $AuCl_4^-$ in W and TPA in DCE (Cell 2). Scan rate; 10 mV s^{-1}. (a) Voltammetry over a restricted potential range (b) extended potential range, where black line; 1st scan, gray lines; 2nd to 9th scan, dotted line; 10th scan. Scan rate; 10 mV s^{-1}.

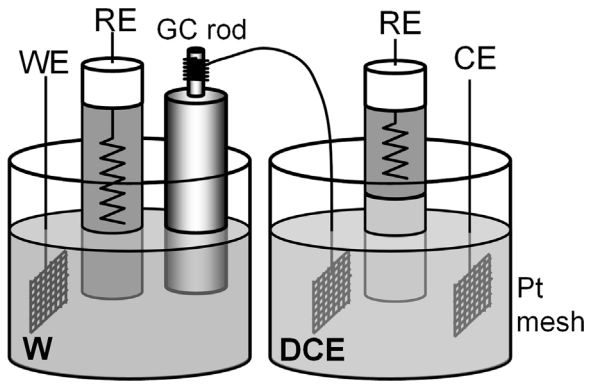

Fig. 3. Two half-cell bridged by solid electrode between $AuCl_4^-$ in W and TPA in DCE.

DCE, decreased with successive potential scans, while, I_{p2}, I_{p3} and I_{n2} increased with repeated potential scanning.

In order to distinguish between ion and electron transfer reactions at I_{n2}, I_{p2} and I_{p3}, electrochemical measurement where the W and DCE phases are separated by a solid electrode [35,36] was carried out as shown in Fig. 3. Here, glassy carbon and platinum wire electrode were used in W and DCE, respectively to connect both phases. Positive and negative current were observed at 0.45 and −0.3 V, corresponding to electron transfer processes: on the basis of the reduction potentials of the Au complex and the TPA (vide infra), these processes are the electrodeposition and stripping of Au as shown in Fig. 4. From the second scan, another current feature corresponding to the formation of the second layer on the Au deposit was observed at 0.26 V, i.e., deposition on the carbon surface give rise to two peaks, on the initial scan a high potential peak (0.45 V) is seen due to the relatively unfavorable energetics of metal deposition on carbon [38]. These peak potentials correlate well with those of the voltammogram recorded at the W/DCE interface (Fig. 2(b)) and therefore suggest that processes I_{p2} and I_{n2} correspond to Au deposition and stripping, respectively. Furthermore, Fig. 4 shows typical features of deposition of a metal at the solid electrode, with a cross-over in the current on the first reduction cycle due to nucleation [17,24,37]. Note that the lower potential deposition peak seen in the bipolar case is not apparent at the W/DCE interface, suggesting it is either obscured by the ion transfer current (I_{p1}/I_{n1}) or Au deposition is occurring more slowly. The latter suggestion may be supported by the lack of "nucleation loop" seen at the W/DCE interface. Consequently, the $AuCl_4^-$ is

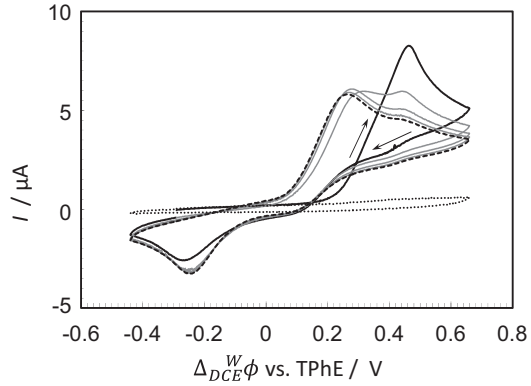

Fig. 4. Charge transfer voltammogram for cell 2 where the two half-cell are bridged by solid electrode between $AuCl_4^-$ in W and TPA in DCE (Cell 2). Glassy carbon and platinum electrode were used as the working electrodes in W and DCE, respectively. Black line; 1st scan, gray lines; 2nd to 4th scans, dotted line; 5th scan. Scan rate; 10 mV s^{-1}.

reduced by TPA not in the bulk DCE phase but at the W/DCE interface, on the transfer of $AuCl_4^-$ to W. In the case of the liquid-liquid interface, there is only one observable deposition peak, whereas a lower potential peak (0.24 V) is seen on subsequent scans, which can be attributed to Au deposition on Au as the following equation;

$$AuCl_4^-{}_{(W)} + 3TPA_{(DCE)} \rightleftharpoons Au + 3TPA^+{}_{(DCE)} + 4Cl^-{}_{(W)} \quad (3)$$

Figure 5 shows the voltammogram recorded at the micro-interface under the same conditions as the macro-interface, Fig. 2, except for the concentration of supporting electrolyte in DCE. In the absence of TPA in DCE, negative current corresponding to the transfer of $AuCl_4^-$ from W to DCE was observed as in curve 1 in Fig. 1. The diffusion coefficient can be calculated from the following equation [31];

$$I_{SS} = 4zFD_W rc_W \quad (4)$$

where I_{ss}, z, F, D_W, r and c_W are the steady state plateau current, the charge number involved in the reaction, the Faraday constant, the diffusion coefficient of the ion in W, the entrance (W side) radius and the concentration of the ion in the bulk of W, respectively. The D calculated (8.3×10^{-6} cm^2 s^{-1}) is similar to that calculated at the macro interface (7.9×10^{-6} cm^2 s^{-1}). In the presence of TPA in DCE, in addition to the negative current corresponding to the transfer of $AuCl_4^-$, a positive current was observed as shown in Fig. 5. The positive current indicates an electron transfer from DCE to W. Here, the shape of the voltammogram did not change with the number of scans. However it was found that the positive current on the forward scan was different from that on the backward scan, whereas minimal hysteresis was seen in the negative current region, corresponding to the transfer of $AuCl_4^-$. This suggests that the reaction associated with the positive current is associated with the nucleation of the Au particles. The data is re-plotted as current normalized for $AuCl_4^-$ concentration. This reveals a decrease in hysteresis as concentration increase, indicating the increased ease of nucleation. The limiting current of the positive process is about twice that of the monovalent $AuCl_4^-$ ion transfer (see insert in Fig. 5). This ratio of positive to negative current is consistent with a three-electron reduction of Au, coupled to the transfer of $AuCl_4^-$ from W to DCE.

Table 2 shows the standard potentials, ΔE^os, of the TPA^+/TPA couple in DCE, and the aqueous $AuCl_4^-$/Au, $AuCl_2^-$/Au and $AuCl_4^-$/$AuCl_2^-$ couples [39]. The oxidation of TPA was investigated voltammetrically and found to give a reversible voltammogram in DCE. The standard electron transfer potential can be calculated from the difference in the standard potentials of TPA^+/TPA in DCE and the $AuCl_4^-$/Au couple in W (0.008 V). Here, ΔE^os obtained on the SSE or NHE scales are converted into those with respect to TPhE

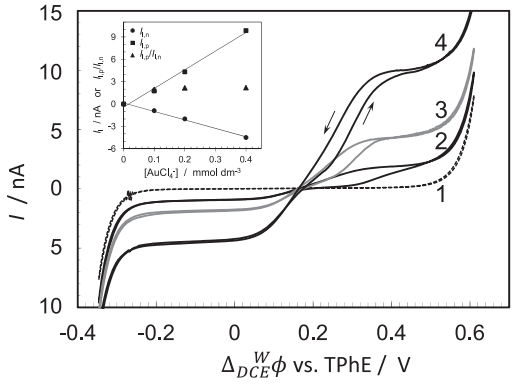

Fig. 5. Charge transfer voltammogram at the micro-interface between $AuCl_4^-$ in W and TPA in DCE (Cell 3). Curves 1 to 5 are 0, 0.1, 0.2, and 0.4 mM $AuCl_4^-$. Scan rate; 10 mV s^{-1}.

Table 2
Standard potential of each redox couple in W or DCE and standard ion transfer potential between W and DCE.

Redox couple	ΔE^o vs.TPhE / V[a]	Ions	$\Delta^w{}_{DCE}\phi^o$ vs. TPhE / V
TPA/TPA^+ in DCE	0.81	$AuCl_4^-$	0.115
$AuCl_4^-$/Au in W	0.802[b]	$AuCl_2^-$	0.026
$AuCl_2^-$/Au in W	0.954[b]		
$AuCl_4^-$/$AuCl_2^-$ in W	0.73[b]		

[a] Converted from SSE or NHE,
[b] ref [39].

at the W/DCE interface [40]. Although the electron transfer reaction was irreversible, the mid-point potential under the condition of Fig. 2(b) was estimated to be approximately 0.07 V, which indicates the electron transfer reaction overlaps with the transfer of $AuCl_4^-$ ion between W and DCE.

3.1.2. *Voltammetry of Au deposition using $AuCl_4^-$ dissolved in DCE*

Before the measurement of the voltammogram in the presence of TPA, a voltammogram in the absence of TPA was recorded as shown in Fig. 6(a). The mid-point potential determined from the potentials at the positive and negative currents at I_{p1} and I_{n1} in Fig. 6 agreed with that obtained in Fig. 1 and reported previously [4,5,7]. The electrochemical reaction between W and DCE containing $AuCl_4^-$ and TPA was thus investigated for the case of $AuCl_4^-$ initially dissolved in DCE. There is no homogeneous reaction between $AuCl_4^-$ and TPA because of the strong solvent dependence of the reduction potential of the former [7,41]. Specifically, the halide loss associated with $AuCl_4^-$ reduction means the $AuCl_4^-$/Au(0) reduction potential is lowered by ca. 2 V. The cyclic voltammograms changed depending on the number of scans as shown in Fig. 6(b). On scanning from −0.15 V, a clear transfer of

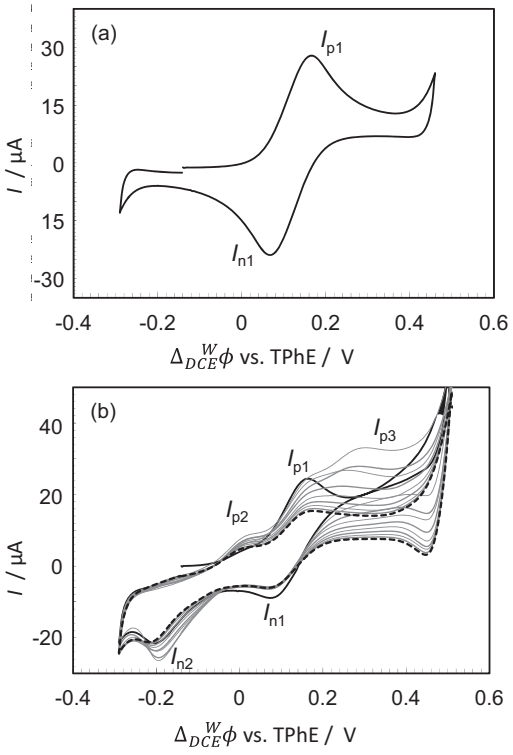

Fig. 6. Ion transfer voltammogram of $AuCl_4^-$ at the macro-interface between W and $AuCl_4^-$ in DCE, i.e. $AuCl_4^-$ initially in DCE phase. Scan rate; 10 mV s^{-1}. (a) absence of TPA, cell 4 (b) presence of TPA (20 mM, Cell 5): Black line; 1st scan, gray lines; 2nd to 4th scans, dotted line; 5th scan.

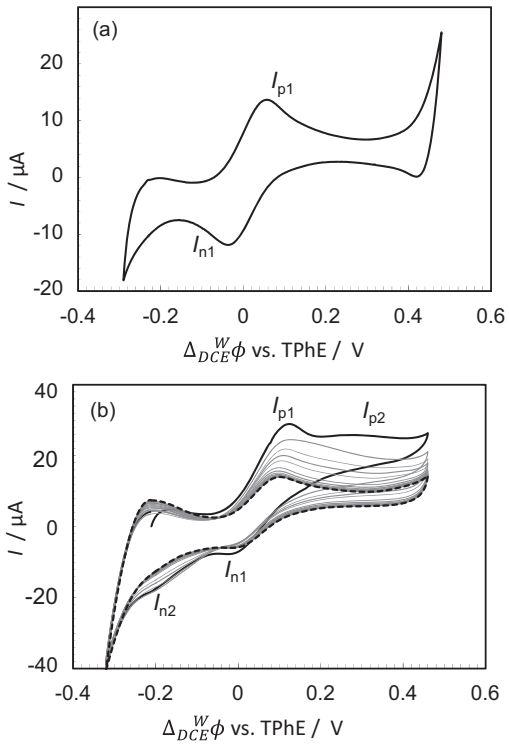

Fig. 7. Ion transfer voltammogram of $AuCl_2^-$ at the macro-interface between W and $AuCl_2^-$ in DCE. Scan rate; 10 mV s^{-1}. (a) in the absence of TPA (Cell 6); (b) with TPA in DCE (Cell 7): black line; 1st scan, gray line; 2nd to 9th scans, dotted line; 10th scan.

$AuCl_4^-$ between W and DCE was observed, which gave a different second voltammogram from that measured when dissolving $AuCl_4^-$ into W instead of DCE (Fig. 2(b)). From the second scan, positive and negative current peaks were observed at 0.35 V and −0.2 V, corresponding to the electron transfer for the redox equilibrium between $AuCl_4^-$ and Au(0). Those potentials are close to those obtained in the analogous cell where $AuCl_4^-$ was initially present in W (Fig. 2(b)). However, the electron transfer current at 0.35 V for the deposition of Au(0) in Fig. 6(b) is clearly higher than that in Fig. 2(b), which must reflect the difference of solvation of the $AuCl_4^-$ transferred from DCE compared to those initially present in W. $AuCl_4^-$ transferring from DCE to W would be immediately reduced to Au(0) at the interface by TPA in DCE, based on the potentials reported in Table 2. By scanning 10 times, the current for the transfer of $AuCl_4^-$, as well as that for the electron transfer, decreased as a result of the irreversible deposition reaction.

3.1.3. Charge transfer voltammetry between W and DCE containing $AuCl_2^-$ and TPA

Cyclic voltammograms were measured for the transfer of $AuCl_2^-$ between W and DCE as shown in Fig. 7(a). Interestingly, in spite of conventional wisdom suggesting $AuCl_2^-$ should disproportionate rapidly in aqueous solution [42], a reversible voltammogram for the transfer of $AuCl_2^-$ from W to DCE was observed(Eq. (5)).

$$AuCl_2^{-}{}_{(DCE)} \rightleftharpoons AuCl_2^{-}{}_{(W)} \quad (5)$$

In the presence of TPA in DCE, voltammograms such as that shown in Fig. 7(b) were recorded. Again because of the solvation effects on reduction [7], $AuCl_2^-$ did not react spontaneously with TPA in DCE. In addition to the $AuCl_2^-$ transfer peaks at 0.08 V, new voltammetric features were observed at 0.2 V on the first scan, with a small negative current seen at −0.2 V. The new features were observed to grow at the expense of the $AuCl_2^-$ transfer peaks and are attributed to Au deposition and stripping at the W/DCE interface:

$$AuCl_2^{-}{}_{(W)} + TPA_{(DCE)} \rightleftharpoons Au + TPA^{+}{}_{(DCE)} + 2Cl^{-}{}_{(W)} \quad (6)$$

The chemical behavior of $AuCl_2^-$ in the presence of TPA is similar to that of $AuCl_4^-$ except that the reversible ion transfer peak (I_{n1}) is smaller in the $AuCl_2^-$ case, and the electron transfer peak (I_{p2}) is enhanced, indicating the higher reactivity of $AuCl_2^-$. After electrolysis at 0.3 V for 2 hours, particle deposition was observed via TEM.

Table 3
Electrochemical deposition experimental by changing applied potential (E_{app}) and duration time (t_{app}) under the condition of Cell 5. Q is the charge.

Batch No.	E_{app} vs. TPhE / V	t_{app} /min	Q /mC
1	0.16	30	6.76
2	0.21	30	12.3
3	0.26	30	18.7
4	0.31	30	27.1
5	0.16	60	12.1
6	0.21	60	22.4

3.2. Effect of electrolysis conditions on Au nanoparticle formation at the liquid/liquid interface

The electrochemical deposition conditions were varied to determine if control over the nanoparticles' mean size and/or density occurred on changing the applied potential (E_{app}) and electrolysis time (t_{app}). Experimental conditions are summarized in Table 3. In this study, W containing 10 mM HCl and DCE containing 0.5 mM $TOA^+AuCl_4^-$, 20 mM TPA and 10 mM TOA^+TFPB^- (Cell 5) was employed. The TOA^+ can act as a capping agent for the Au deposit [28].

Electrolysis at E_{app} = 0.21 V and t_{app} = 30 min produced particles in the size range 3–7 nm as shown in Fig. 8 (a). However, the total amount of particles was much lower than formed under the other conditions employed, although a significant deposition current was observed at the potential in Fig. 6(b). E_{app} = 0.26 V and t_{app} = 30 min, gave many 3 nm diameter particles in addition to the lesser number of particles in the 2–7 nm range shown in Fig. 8 (b). At E_{app} = 0.31 V, particles of 3–5 nm diameter were mainly observed (Fig. 8 (c)). The average size of those particles at E_{app} = 0.31 V seemed to be larger than E_{app} = 0.21 and 0.26 V. Particles around 50 nm in diameter were observed at E_{app} = 0.36 V and t_{app} = 30 min in addition to the ca. 10 nm diameter particles. The size of particles produced was not closely correlated with the applied potential, although there was a tendency to form larger particles, at more positive potential. The ex-situ nature of the TEM analysis makes comparative evaluation of particle number difficult but the exponential increase in current with potential in the potential range of Fig. 6(b) (compare with Fig. 5) therefore suggests that the main change with potential is likely with respect to the number of particles formed. Table 3 gives the charge passed for the different E_{app} and t_{app}. No particles were observed from TEM samples obtained at potentials below the onset of I_{p3} in Fig. 6(b) (specifically E_{app} = 0.16 V and t_{app} = 30 min). Finally, longer term electrolysis was carried out using E_{app} = 0.16 and 0.21 V for t_{app} = 60 min. Fig. 8 (d) shows the result from E_{app} = 0.21 V and t_{app} = 60 min. Larger particles having diameter in the range 4–8 nm were observed compared with those formed at the same potential and t_{app} = 30 min. Moreover there was evidence of particle aggregation in the case of the longer t_{app} experiments (10–15 nm). Consequently, synthesis of particle with diameters less than 10 nm requires E_{app} = 0.21–0.31 V and t_{app} = 30 min under the experimental conditions employed here.

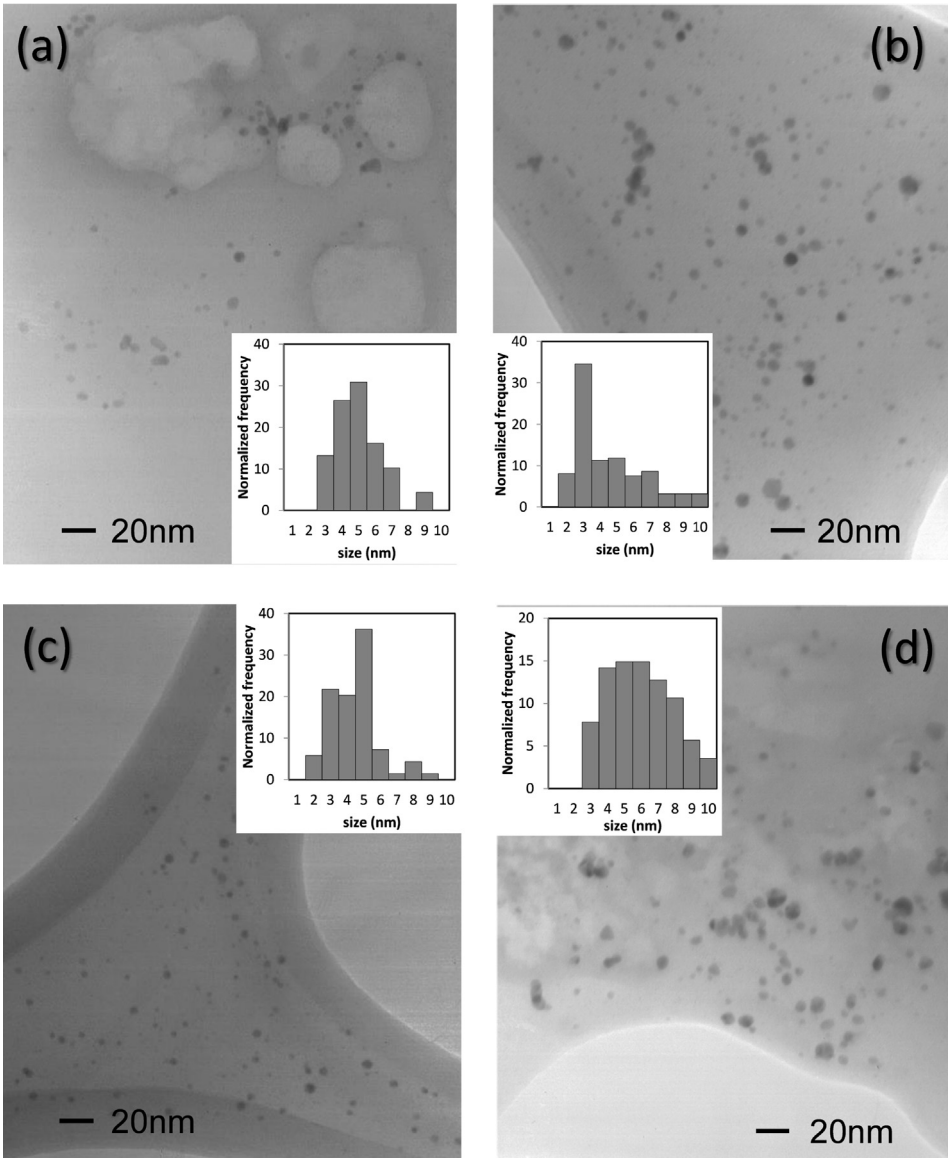

Fig. 8. TEM image of DCE after the electrolysis at (a) E_{app} = 0.21 V and t_{app} = 30 min, (b) E_{app} = 0.26 V and t_{app} = 30 min, (c) E_{app} = 0.31 V and t_{app} = 30 min, and (d) E_{app} = 0.21 and t_{app} = 60 min which were carried out under the condition of Cell 5.

4. Conclusions

It has been found that Au deposit was formed at the interface from the simultaneous reduction of $AuCl_4^-$ or $AuCl_2^-$ in W and concomitant oxidation of TPA as a reductant in DCE. Ion transfer voltammetry indicated that $AuCl_2^-$ is stable, at least on the second timescale, in aqueous solution. The formation of Au nanoparticle with diameters less than 10 nm was more sensitive to time of electrolysis than the applied potential.

Acknowledgements

The authors thank Prof. M. Oyama (Kyoto Univ.) and Dr. Y. Gründer (Univ. of Manchester) for fruitful discussions. This research was partly supported by The Kyoto University Foundation and EPSRC (grant reference EP/H047786/1).

References

[1] M. Faraday, Experimental Relations of Gold (and other metals) to Light, Phil. Trans. Royal Soc 147 (1857) 145.
[2] J. Eastoe, M.J. Hollamby, L. Hudson, Recent advances in nanoparticle synthesis with reversed micelles, Adv. Colloid Interface Sci. 128–130 (2006) 5.
[3] R.A.W. Dryfe, Modifying the liquid/liquid interface: pores, particles and deposition, Phys. Chem. Chem. Phys. 8 (2006) 1869.
[4] Y. Cheng, D.J. Schiffrin, Electrodeposition of metallic gold clusters at the water/1,2-dichloroethane interface, J. Chem. Soc., Faraday Trans. 92 (1996) 3865.
[5] R. Knake, A.W. Fahmi, S.A.M. Tofail, J. Clohessy, M. Mihov, V.J. Cunnane, Electrochemical nucleation of gold nanoparticles in a polymer film at a liquid-liquid interface, Langmuir 21 (2005) 1001.
[6] A.I. Campbell, R.A.W. Dryfe, M.D. Haw, Deposition and Aggregation of Au at the Liquid/Liquid Interface, Anal. Sci. 25 (2009) 307.
[7] Y. Gründer, H.L.T. Ho, J.F.W. Mosselmans, S.L.M. Schroeder, R.A.W. Dryfe, Inhibited and enhanced nucleation of gold nanoparticles at the water|1,2-dichloroethane interface, Phys. Chem. Chem. Phys. 13 (2011) 15681.
[8] I. Kaminska, M. Jonsson-Niedziolka, A. Kaminska, M. Pisarek, R. Holyst, M. Opallo, J. Niedziolka-Jonsson, Electrodeposition of Well-Adhered Multifarious Au Particles at a Solid|Toluene|Aqueous Electrolyte Three-Phase Junction, J. Phys. Chem. C 116 (2012) 22476.

[9] K. Lepkova, J. Clohessy, V.J. Cunnane, Electrodeposition of metal-based nanocomposites at a liquid-liquid interface controlled via the interfacial Galvani potential difference, Electrochim. Acta 53 (2008) 6273.
[10] K. Lepkova, J. Clohessy, V.J. Cunnane, The pH-controlled synthesis of a gold nanoparticle/polymer matrix via electrodeposition at a liquid-liquid interface, J Phys-Condens Mat. 19 (2007) 375106.
[11] M. Guainazzi, G. Silvestri, G. Serravalle, Electrochemical metallization at the liquid-liquid interfaces of non-miscible electrolytic solutions, J. Chem. Soc., Chem. Comm. (1975) 200.
[12] C. Johans, R. Lahtinen, K. Kontturi, D.J. Schiffrin, Nucleation at liquid | liquid interfaces: electrodeposition without electrodes, J. Electroanal. Chem 488 (2000) 99.
[13] C. Johans, P. Liljeroth, K. Kontturi, Electrodeposition at polarisable liquid|liquid interfaces: The role of interfacial tension on nucleation kinetics, Phys. Chem. Chem. Phys 4 (2002) 1067.
[14] D. Izquierdo, A. Martinez, A. Heras, J. Lopez-Palacios, V. Ruiz, R.A.W. Dryfe, A. Colina, Spatial Scanning Spectroelectrochemistry. Study of the Electrodeposition of Pd Nanoparticles at the Liquid/Liquid Interface, Anal. Chem 84 (2012) 5723.
[15] M. Platt, R.A.W. Dryfe, E.P.L. Roberts, Structural and electrochemical characterisation of Pt and Pd nanoparticles electrodeposited at the liquid/liquid interface, Electrochim. Acta 49 (2004) 3937.
[16] J.J. Nieminen, I. Hatay, P. Ge, M.A. Méndez, L. Murtomäki, H.H. Girault, Hydrogen evolution catalyzed by electrodeposited nanoparticles at the liquid/liquid interface, Chem. Comm 47 (2011) 5548.
[17] A. Trojanek, J. Langmaier, Z. Samec, Random nucleation and growth of Pt nanoparticles at the polarised interface between two immiscible electrolyte solutions, J. Electroanal. Chem 599 (2007) 160.
[18] C. Johans, J. Clohessy, S. Fantini, K. Kontturi, V.J. Cunnane, Electrosynthesis of polyphenylpyrrole coated silver particles at a liquid-liquid interface, Electrochem. Comm 4 (2002) 227.
[19] J. Guo, T. Tokimoto, R. Othman, P.R. Unwin, Formation of mesoscopic silver particles at micro- and nano-liquid/liquid interfaces, Electrochem. Comm 5 (2003) 1005.
[20] V. Mirceski, R. Gulaboski, Simple electrochemical method for deposition and voltammetric inspection of silver particles at the liquid-liquid interface of a thin-film electrode, J. Phys. Chem. B 110 (2006) 2812.
[21] F. Li, M. Edwards, J.D. Guo, P.R. Unwin, Silver Particle Nucleation and Growth at Liquid/Liquid Interfaces: A Scanning Electrochemical Microscopy Approach, J. Phys. Chem. C 113 (2009) 3553.
[22] U. Hasse, G.J. Palm, W. Hinrichs, J. Schäfer, F. Scholz, The growth of single crystal silver wires at the nitrobenzene|water interface, Phys. Chem. Chem. Phys 13 (2011) 12254.
[23] R.A.W. Dryfe, A.O. Simm, B. Kralj, Electroless deposition of palladium at bare and templated liquid/liquid interfaces, J. Am. Chem. Soc 125 (2003) 13014.
[24] C. Johans, K. Kontturi, D.J. Schiffrin, Nucleation at liquid vertical bar liquid interfaces: galvanostatic study, J. Electroanal. Chem 526 (2002) 29.
[25] M. Platt, R.A.W. Dryfe, E.P.L. Roberts, Controlled deposition of nanoparticles at the liquid-liquid interface, Chem. Comm. (2002) 2324.
[26] Y. Gründer, J.F.W. Mosselmans, S.L.M. Schroeder, R.A.W. Dryfe, In Situ Spectroelectrochemistry at Free-Standing Liquid–Liquid Interfaces: UV–vis Spectroscopy, Microfocus X-ray Absorption Spectroscopy, and Fluorescence Imaging, J. Phys. Chem. C 117 (2013) 5765.
[27] B.L. Cushing, V.L. Kolesnichenko, C.J. O'Connor, Recent advances in the liquid-phase syntheses of inorganic nanoparticles, Chem. Rev 104 (2004) 3893.
[28] M.T. Reetz, W. Helbig, Size-selective Synthesis of Nanostructured Trasition-metal Crusters, J. Am. Chem. Soc 116 (1994) 7401.
[29] H. Bonnemann, W. Brijoux, R. Brinkmann, E. Dinjus, T. Joussen, B. Korall, Formation of Colloidal Transition-metals in Organic Phases and Their Application in Catalysis, Angew. Chem., Int. Ed., 30 (1991) 1312.
[30] G. Taylor, H.H.J. Girault, Ion Transfer-Reactions across a Liquid Liquid Interface Supported on a Micropipette Tip, J. Electroanal. Chem. 208 (1986) 179.
[31] M.D. Osborne, Y. Shao, C.M. Pereira, H.H. Girault, Micro-Hole Interface for the Amperometric Determination of Ionic Species in Aqueous-Solutions, J. Electroanal. Chem 364 (1994) 155.
[32] H. Ohde, A. Uehara, Y. Yoshida, K. Maeda, S. Kihara, Some factors in the voltammetric measurement of ion transfer at the micro aqueous vertical bar organic solution interface, J. Electroanal. Chem 496 (2001) 110.
[33] A.J. Olaya, M.A. Méndez, F. Cortes-Salazar, H.H. Girault, Voltammetric determination of extreme standard Gibbs ion transfer energy, J. Electroanal. Chem 644 (2010) 60.
[34] A.J. Parker, Protic-dipolar Aprotic Solvent Effects on Rates of Biomolecular Reactions, Chem. Rev 69 (1969) 1.
[35] H. Hotta, N. Akagi, T. Sugihara, S. Ichikawa, T. Osakai, Electron-conductor separating oil-water (ECSOW) system: a new strategy for characterizing electron-transfer processes at the oil/water interface, Electrochem. Comm 4 (2002) 472.
[36] H. Hotta, S. Ichikawa, T. Sugihara, T. Osakai, Clarification of the mechanism of interfacial electron-transfer reaction between ferrocene and hexacyanoferrate(III) by digital simulation of cyclic voltammograms, J. Phys. Chem. B 107 (2003) 9717.
[37] M. Platt, R.A.W. Dryfe, E.P.L. Roberts, Electrodeposition of palladium nanoparticles at the liquid-liquid interface using porous alumina templates, Electrochim. Acta 48 (2003) 3037.
[38] U. Schmidt, M. Donten, J.G. Osteryoung, Gold electrocrystallization on carbon and highly oriented pyrolytic graphite from concentrated solutions of LiCl, J. Electrochem. Soc 144 (1997) 2013.
[39] K.E. Heusler, W.J. Lorenz, in: A.J. Bard, R. Parsons, J. Jordan (Eds.), Standard Potentials in Aqueous Solution, Marcel Dekker, New York, 1985, pp. 391–412.
[40] H. Shiba, K. Maeda, N. Ichieda, M. Kasuno, Y. Yoshida, O. Shirai, S. Kihara, Voltammetric study on the electron transport through a bilayer lipid membrane containing neutral or ionic redox molecules, J. Electroanal. Chem 556 (2003) 1.
[41] E.T. Seo, R.F. Nelson, J.M. Fritsch, L.S. Marcoux, D.W. Leedy, R.N. Adams, Anodic Oxidation Pathways of Aromatic Amines. Electrochemical and Electron Paramagnetic Resonance Studies, J. Am. Chem. Soc. 88 (1966) 3498.
[42] C.H. Gammons, Y.M. Yu, A.E. WiliamsJones, The disproportionation of gold(I) chloride complexes at 25 to 200 degrees C, Geochim. Cosmochim. Acta 61 (1997) 1971.